



Cite this: *RSC Adv.*, 2017, 7, 19584

Single-phase white-emitting phosphors $\text{Ba}_3\text{Ce}_{(1-x-y)}(\text{PO}_4)_3:\text{xTb}^{3+}, \text{yMn}^{2+}$ and $\text{Ba}_3\text{Ce}_{(1-x-z)}(\text{PO}_4)_3:\text{xTb}^{3+}, \text{zSm}^{3+}$: structure, luminescence, energy transfer and thermal stability

 Shuchao Xu, Zhijun Wang, * Panlai Li, * Ting Li, Qiongyu Bai, Jiang Sun and Zhiping Yang

A series of $\text{Ba}_3\text{Ce}_{(1-x-y)}(\text{PO}_4)_3:\text{xTb}^{3+}, \text{yMn}^{2+}$ and $\text{Ba}_3\text{Ce}_{(1-x-z)}(\text{PO}_4)_3:\text{xTb}^{3+}, \text{zSm}^{3+}$ phosphors were synthesized by a high temperature solid-state reaction. X-ray diffraction, luminescence and decay curves were used to characterize the phosphors. All the synthesized phosphors crystallized in the cubic unit cell with $I\bar{4}3d$ space group. Energy can be transferred from Ce^{3+} to $\text{Tb}^{3+}/\text{Mn}^{2+}/\text{Sm}^{3+}$ in $\text{Ba}_3\text{Ce}_{(1-x)}(\text{PO}_4)_3:\text{xTb}^{3+}$, $\text{Ba}_3\text{Ce}_{(1-y)}(\text{PO}_4)_3:\text{yMn}^{2+}$, and $\text{Ba}_3\text{Ce}_{(1-z)}(\text{PO}_4)_3:\text{zSm}^{3+}$ phosphors. Furthermore, the color of these phosphors can turn from cyan to green, blue to red, and cyan to pale pink. When $\text{Ba}_3\text{Ce}(\text{PO}_4)_3$ was co-doped with Tb^{3+} and $\text{Mn}^{2+}/\text{Sm}^{3+}$, Tb^{3+} could also transfer part of its energy to $\text{Mn}^{2+}/\text{Sm}^{3+}$, and more importantly, a white emission can be achieved based on this energy transfer. The phosphors exhibited a good thermal stability, with correlated color temperatures of up to 3301 K, and a quantum efficiency as high as 51.2%. These results revealed that we managed to obtain good white emitting phosphors by co-doping $\text{Ba}_3\text{Ce}(\text{PO}_4)_3$ with Tb^{3+} and $\text{Mn}^{2+}/\text{Sm}^{3+}$.

Received 12th February 2017
Accepted 13th March 2017

DOI: 10.1039/c7ra01766a

rsc.li/rsc-advances

1 Introduction

The extensive application of white light-emitting diodes (LEDs) has attracted significant attention because of their long lifetime, environmental friendliness, high luminescence efficiency and material stability.^{1–3} Traditional white YAG:Ce³⁺ LEDs were fabricated with a blue-chip, which exhibit high correlated color temperature (CCT ~ 7750 K) and poor color rendering index (CRI70 ~ 80).⁴ Therefore, to obtain high-performance white LEDs, other methods have been introduced. One of the methods for achieving white emission is co-doping different ions in a single-phase compound.^{5–7} This can not only overcome the shortcomings of high correlated color temperature and low color rendering index, but also avoid reabsorption in the host.^{8–11} Generally, energy transfer plays an important role in the optical properties of co-doped luminescent materials, from which we can obtain a tunable color or white emission.¹² Among ions, Ce³⁺ can not only emit blue emission, but can also transfer part of its energy to other ions because of its 5d → 4f transition.^{13–17} Moreover, Tb³⁺ ions are widely used as important green activators due to their ⁵D₄ → ⁷F_J transitions (*J* = 6, 5, 4 and 3).^{18,19} Furthermore, Mn²⁺/Sm³⁺ can be acceptors and can produce the red emission components in the host. Thus, it is

possible to obtain a white emission *via* tri-doping Ce³⁺, Tb³⁺ and Mn²⁺/Sm³⁺ in a single-phase compound.

Among many host compounds, eulytite-type orthophosphates of the M₃M^{II}(PO₄)₃ (M^I = Ba, Sr, Ca, and Pb, M^{II} = La, Sc, Y, Bi, and In) type have attracted significant interest for their good optical properties and thermal stability.^{20–24} Ba₃Ce(PO₄)₃ (BCP) is a eulytite-type phosphate, with the advantage of having Ce³⁺ as one of the matrix cations. Thus, the doping concentration of Ce³⁺ is up to 100%, such that Ce³⁺ can transfer a large amount of energy to the co-doping ions in the host.^{25,26} Therefore, in our study, a series of white-emitting Ba₃Ce(PO₄)₃:Tb³⁺/Mn²⁺/Sm³⁺ phosphors were investigated, along with the energy transfer from Ce³⁺ to other activators. Importantly, the white emitting phosphors Ba₃Ce(PO₄)₃:Tb³⁺, Mn²⁺ and Ba₃Ce(PO₄)₃:Tb³⁺, Sm³⁺ exhibited a good thermal stability and correlated color temperatures.

2 Experimental

2.1 Materials and synthesis

A series of $\text{Ba}_3\text{Ce}_{(1-x-y)}(\text{PO}_4)_3:\text{xTb}^{3+}, \text{yMn}^{2+}$ and $\text{Ba}_3\text{Ce}_{(1-x-z)}(\text{PO}_4)_3:\text{xTb}^{3+}, \text{zSm}^{3+}$ phosphors were prepared by a high-temperature solid-state reaction process. The raw materials BaCO₃ (analytical reagents, A.R.), NH₄H₂PO₄ (A.R.), CeO₂ (99.99%), Tb₄O₇ (99.99%), Sm₂O₃ (99.99%) and MnCO₃ (A.R.) were weighed using an electronic scale with a 0.0001 g accuracy. The stoichiometric amounts of raw materials were thoroughly

College of Physics Science & Technology, Hebei Key Lab of Optic-electronic Information and Materials, Hebei University, Baoding 071002, China. E-mail: wangzj1998@126.com; li_panlai@126.com



mixed and ground using an agate mortar and pestle for more than 30 min until they became uniformly distributed. Then, the obtained material was transferred into an alumina crucible and sintered at 1150 °C for 4 h in a reductive atmosphere (20% H₂ + 80% N₂). After sintering, samples were cooled down to room temperature and then ground again into a powder for subsequent use.

2.2 Material characterization

X-ray diffraction (XRD) patterns of the as-synthesized samples were obtained to determine the crystal structure, using a D/max- α with Cu K α radiation at 40 kV and 40 mA. XRD patterns, which were analyzed by Rietveld refinement, were acquired at the step size of 0.05° with a counting time of 2 s per step. Findit software and Crystallmaker software were used for identifying the structure. Spectral properties were analyzed *via* a F-4600 spectrofluorometer equipped with a 450 W Xe lamp. Temperature-dependent luminescence properties were measured *via* the same spectrophotometer, which was assembled with a TAP-02 high-temperature fluorescence controller. The Commission International de l'Eclairage (CIE) chromaticity coordinates of the samples were measured by a PMS-80 UV-VIS-NEAR IR spectra analysis system. Decay curves of Tb³⁺/Sm³⁺/Mn²⁺ were obtained using a 450 W Xe lamp as the excitation source (HORIBA, FL-1057). Decay curves of Ce³⁺ were obtained using a nona LED (370 nm) as the excitation source. Furthermore, particle morphology was investigated by scanning electron microscopy (SEM), and images were obtained using Nova NanoSEM 650 at the accelerating voltage of 10 kV.

3 Results and discussion

3.1 Phase formation

The phase purity of our phosphors was evaluated by X-ray diffraction. Fig. 1 exhibits the XRD patterns of representative phosphors as well as the standard card of Ba₃La(PO₄)₃ for comparison. It can be found that all the diffraction peaks of the samples can be exactly assigned to the pure cubic phase Ba₃-La(PO₄)₃ (JCPDS 85-2448). No other phase or impurity were detected, indicating that the doped ions cannot induce significant changes in the crystal structure. In other words, our samples were obtained without any heterogeneous phase. The SEM images of BCP, BCP:0.07Tb³⁺, BCP:0.07Tb³⁺,0.07Mn²⁺ and BCP:0.07Tb³⁺,0.07Sm³⁺ are shown in the lower part of Fig. 1. It was found that the samples consisted of aggregated particles with a sphere-like morphology of an average size of 5–10 μ m. A micrometer-size of the phosphor particles is essential for high luminescence, and the synthesized phosphors exhibit a particle size in the micrometer range, and hence, they can exhibit a good luminescence.

For the purpose of further elucidating the crystal structure of the samples, we analyzed the XRD patterns by Rietveld refinements, as represented in Fig. 2(a–e). The multiplication sign denotes the XRD pattern of the samples, the red lines represent the corresponding Rietveld refinement, and the blue line represents the residuals. The refinement results, as presented

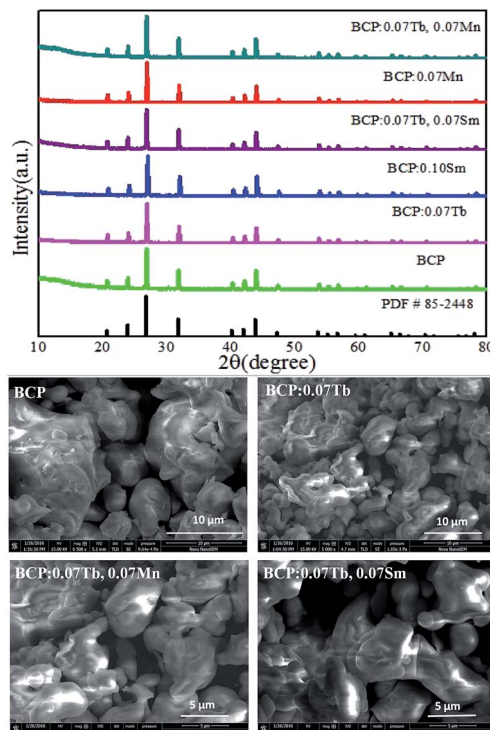


Fig. 1 X-ray diffraction patterns of BCP; BCP:0.07Tb; BCP:0.10Sm; BCP:0.07Tb,0.07Sm; BCP:0.07Mn; BCP:0.07Tb,0.07Mn and JCPDS card no. 85-2448, corresponding to Ba₃La(PO₄)₃. Below are the SEM images of the samples.

in Table 1, further demonstrate that the phosphors are single-phase without any impurity or secondary phases. As shown in Fig. 2(f), (I) is the crystal structure of Ba₃La(PO₄)₃ in a cubic system with space group $I\bar{4}3d$ of the unit cell, and (II) and (III) are the coordination environments of the P⁵⁺ and Ba²⁺/La³⁺/Ce³⁺ sites. In the structure, each P⁵⁺ is surrounded by 8 O²⁻ anions to form an octahedron with four long P–O distances of 1.501 Å and four short P–O distances of 1.488 Å. Each Ba²⁺ is coordinated with 18 non-equidistant oxygens at the distance ranging from 2.704 Å to 2.973 Å.

3.2 Luminescence properties

The inset of Fig. 3 shows the emission and excitation spectra of BCP. Under excitation at 325 nm, BCP shows a broad-band blue emission ranging from 350 to 550 nm, centered at 387 nm. This emission is attributed to the transition of Ce³⁺ from the 5d excited state to the 4f ground state. The corresponding excitation spectrum (monitored at 387 nm) covering the range of 200–350 nm is attributed to the 4f → 5d transition of Ce³⁺. Fig. 3 shows the decay curve of BCP, and the luminescence decay time can be calculated by the following formula:²⁷

$$\tau = \left(\int I(t) dt \right) / \left(\int I(t) dt \right) \quad (1)$$

where $I(t)$ represents the luminescence intensity at a time t , t is the time, and τ is the lifetime. The calculated decay time is



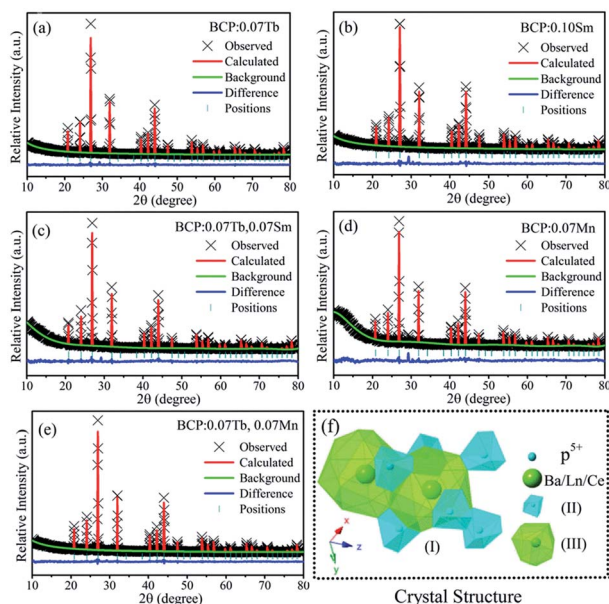


Fig. 2 (a)–(e) Rietveld refinements of BCP:0.07Tb; BCP:0.10Sm; BCP:0.07Tb,0.07Sm; BCP:0.07Mn and BCP:0.07Tb,0.07Mn; (f) crystal structure of $\text{Ba}_3\text{La}(\text{PO}_4)_3$.

shown in Fig. 3. Moreover, the measured quantum efficiency of the host was 55.3%.

To study whether there is energy transfer from Ce to Tb, we studied the emission and excitation spectra of BCP and BTP ($\text{Ba}_3\text{Tb}(\text{PO}_4)_3$), as shown in Fig. 4. For BTP, the excitation spectrum monitored at 551 nm contains two broad bands and many other bands, which are attributed to $f \rightarrow d$ and $f \rightarrow f$ transitions in Tb^{3+} . The emission spectrum at 377 nm excitation consists of several bands from 480 to 650 nm, attributed to $^5\text{D}_4 \rightarrow ^7\text{F}_j$ ($j = 6, 5, 4, 3$) transitions in Tb^{3+} . Moreover, the results show that there is an overlap between the emission spectrum of BCP and the excitation spectrum of BTP. Therefore, we hypothesized that Ce^{3+} might transfer its energy to Tb^{3+} in eulytite-type phosphates. Fig. 4(c) and (d) depict the emission and excitation spectra of BCP:0.03 Tb^{3+} and BTP:0.03 Ce^{3+} , respectively. It can be clearly seen that the excitation spectra monitored at 551 nm for BCP:0.03 Tb^{3+} is similar to the excitation spectrum monitored at 387 nm for BCP. Moreover, both emission spectra ($\lambda_{\text{ex}} = 325$ nm) of the doped BCP and BTP display the characteristic peaks of Ce^{3+} and Tb^{3+} . Thus, we

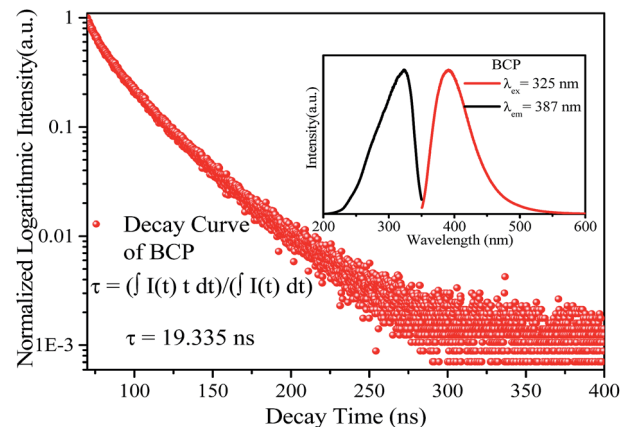


Fig. 3 Decay curve of BCP, the inset shows the emission and excitation spectra of BCP.

synthesized BCP: $x\text{Tb}^{3+}$ to further explore whether energy transfer occurs. As depicted in Fig. 4(e), the emission spectra ($\lambda_{\text{ex}} = 325$ nm) of all samples contain both Ce^{3+} and Tb^{3+} emission bands. In addition, as shown in Fig. 4(f), the emission intensity of Ce^{3+} monotonously decreases as the Tb^{3+} concentration increases, which evidences the occurrence of energy transfer from Ce^{3+} to Tb^{3+} . Importantly, the emission color shifts from cyan to green as Tb^{3+} concentration increases in BCP: $x\text{Tb}^{3+}$.

To obtain white emission, there should be a red component in the emission spectrum of the phosphor. Thus, we first synthesized a series of $\text{Ce}^{3+}/\text{Mn}^{2+}$ and $\text{Ce}^{3+}/\text{Sm}^{3+}$ co-doped phosphors. To investigate the luminescence characteristics, the emission and excitation spectra were obtained and are shown in Fig. 5(a). The excitation spectra of BCP:0.10Sm monitored at 606 nm and 387 nm are similar in the range from 200 to 370 nm. The differences from 370 to 550 nm is due to the transitions of Sm^{3+} . Furthermore, the excitation spectrum monitored at 606 nm has a broad overlap with the emission spectrum excited at 325 nm of BCP. Thus, energy transfer from Ce^{3+} to Sm^{3+} ions in BCP:0.10 Sm^{3+} may take place. Moreover, we synthesized a series of BCP: $z\text{Sm}$, and their spectra at 325 nm excitation contain both Ce^{3+} and Sm^{3+} emission bands, as shown in Fig. 5(b). The inset is the enlarged spectra from 560 to 680 nm centered at 565, 606 and 650 nm, which are assigned to the $^4\text{G}_{5/2} \rightarrow ^6\text{H}_{5/2}$, $^6\text{H}_{7/2}$ and $^6\text{H}_{9/2}$ transitions of Sm^{3+} , respectively. As depicted in Fig. 5(c), the emission intensity of Ce^{3+} decreases as the Sm^{3+}

Table 1 XRD refinement results of the samples

	BCP:0.07Tb	BCP:0.07Mn	BCP:0.10Sm	BCP: 0.07Tb,0.07Mn	BCP: 0.07Tb,0.07Sm
χ^2	2.850	1.704	2.058	1.983	1.587
R_p	8.49%	7.48%	8.44%	8.04%	7.30%
R_{wp}	12.67%	7.84%	10.18%	11.16%	7.15%
$a = b = c$	10.500	10.512	10.520	10.501	10.514
Cell volume/ \AA^3	1157.158	1161.657	1164.305	1158.073	1162.349
$\alpha = \beta = \gamma$	90°	90°	90°	90°	90°
Z	4	4	4	4	4
Space group	$I\bar{4}3d$	$I\bar{4}3d$	$I\bar{4}3d$	$I\bar{4}3d$	$I\bar{4}3d$



concentration increases. Moreover, the emission intensity of Sm^{3+} steeply increases until it reaches a maximum at $z = 0.10$. Then, due to concentration quenching, the emission intensity gradually decreases, which further evidences the energy transfer from Ce^{3+} to Sm^{3+} ions. As a result of the energy transfer, in the co-doped BCP:zSm^{3+} , the color can turn from cyan to pale pink.

In addition, as shown in Fig. 5(d), the excitation spectra of Mn^{2+} ion monitored at 606 nm is exactly the same to that of Ce^{3+} ion monitored at 387 nm in BCP:0.07Mn^{2+} . This implies that energy transfer from Ce^{3+} to Mn^{2+} ions should also occur. To further prove this hypothesis, the emission spectra of BCP:yMn^{2+} at 325 nm excitation were obtained and are shown in Fig. 5(e). There are two broad emission bands, the one from 350 to 500 nm is attributed to the $5d \rightarrow 4f$ transition in Ce^{3+} , and the other band, from 550 nm to 700 nm is attributed to the ${}^4\text{T}_1({}^4\text{G}) \rightarrow {}^6\text{A}_1({}^6\text{S})$ spin-forbidden transition of Mn^{2+} .^{28,29} The variation in emission intensity with different Mn^{2+} contents, depicted in Fig. 5(f), shows that the intensity of Ce^{3+} gradually decreases, whereas the intensity of Mn^{2+} first increases, and then decreases as the concentration of Mn^{2+} increases due to concentration quenching. Thus, these results evidence the occurrence of energy transfer from Ce^{3+} to Mn^{2+} ions. As a result

of the energy transfer, in the co-doped BCP:yMn^{2+} , the color can change from blue to red.

For the purpose of further demonstrating the energy transfer in BCP:xTb^{3+} , BCP:yMn^{2+} and BCP:zSm^{3+} , Fig. 6 presents the decay curves of the abovementioned samples. Fig. 6(a–c) show the decay curves of Ce^{3+} in BCP:xTb^{3+} , BCP:yMn^{2+} , and BCP:zSm^{3+} monitored at 387 nm upon 325 nm excitation. Moreover, Fig. 6(d–f) show the corresponding decay curves of Tb^{3+} ($\lambda_{\text{em}} = 551 \text{ nm}$, $\lambda_{\text{ex}} = 377 \text{ nm}$), Mn^{2+} ($\lambda_{\text{em}} = 606 \text{ nm}$, $\lambda_{\text{ex}} = 387 \text{ nm}$), and Sm^{3+} ($\lambda_{\text{em}} = 606 \text{ nm}$, $\lambda_{\text{ex}} = 387 \text{ nm}$) in BCP:xTb^{3+} , BCP:yMn^{2+} , and BCP:zSm^{3+} , respectively. The decay time values of Ce, Tb, Mn, and Sm in the corresponding samples, as shown in Table 2, were calculated according to formula (1).

From Table 2, it can be observed that the decay time values of Ce^{3+} in doped BCP are all lower than the decay time of Ce^{3+} in BCP, which is shown in Fig. 3. Moreover, the decay time decreases as the amount of doping $\text{Tb}^{3+}/\text{Mn}^{2+}/\text{Sm}^{3+}$ in BCP increases. For Tb^{3+} in BCP:xTb^{3+} , Mn^{2+} in BCP:yMn^{2+} and Sm^{3+} in BCP:zSm^{3+} , the decay time increases first and then rapidly decreases as the amount of doping ions increases, which is attributed to the energy transfer and concentration quenching effect, respectively. In other words, when the ion content is higher, the distance between ions becomes smaller and energy can transfer from Ce to Tb/Mn/Sm. Thus, the increase in decay time is a result of two aspects: one is the increasing ions

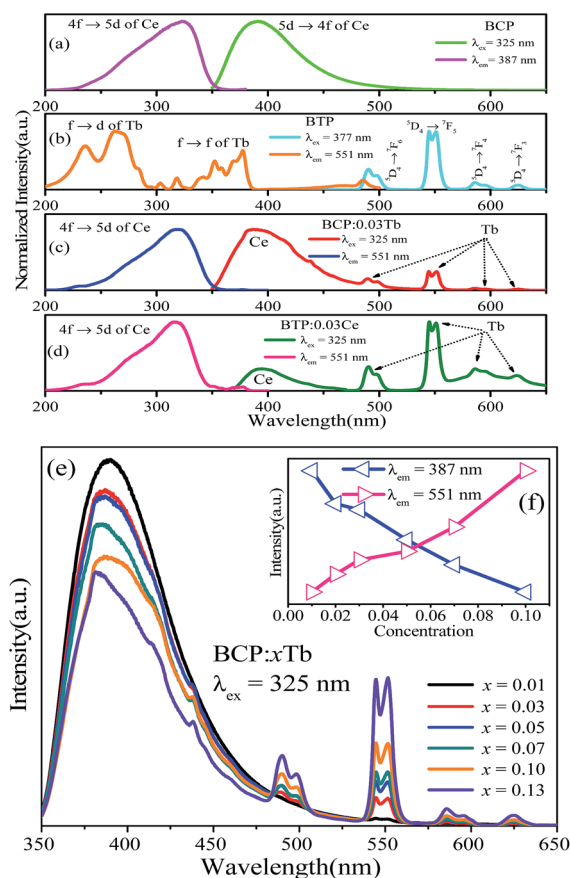


Fig. 4 (a)–(d) Emission and excitation spectra of BCP, BTP, BCP:0.03Tb , and BTP:0.03Ce . (e) Emission spectra of BCP:xTb ($\lambda_{\text{ex}} = 325 \text{ nm}$) ($x = 0.01$ – 0.13). (f) Ce^{3+} and Tb^{3+} intensity versus Tb^{3+} concentration in BCP:xTb .

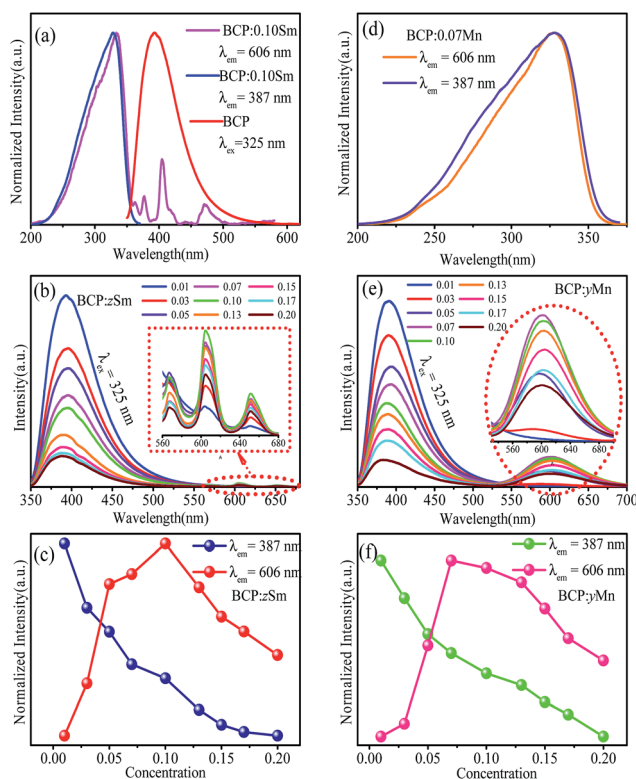


Fig. 5 (a) Emission spectra of BCP:0.10Sm and excitation spectrum of BCP. (b) Emission spectra of BCP:zSm . (c) Variation in the emission intensity with different z . (d) Emission spectra of BCP:0.07Mn . (e) Emission spectra of BCP:yMn . (f) Variation in the emission intensity with different y .

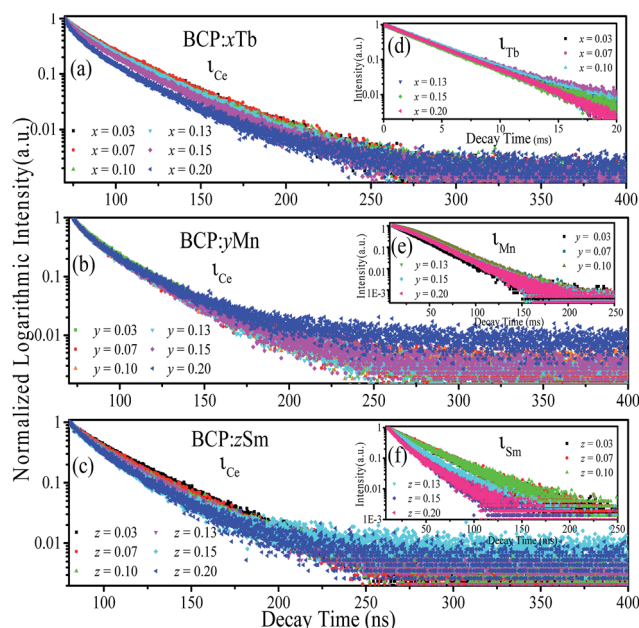


Fig. 6 (a–c) Decay curves of Ce^{3+} in BCP: $x\text{Tb}$, BCP: $y\text{Mn}$, and BCP: $z\text{Sm}$. (d–f) Decay curves of Tb^{3+} in BCP: $x\text{Tb}$, Mn^{2+} in BCP: $y\text{Mn}$, and Sm^{3+} in BCP: $z\text{Sm}$.

concentration and the other is the energy transfer from Ce to the doping ions. However, when the concentration of doping ions is high enough, concentration quenching occur. Thus, the results once again confirm the energy transfer from Ce^{3+} to $\text{Tb}^{3+}/\text{Mn}^{2+}/\text{Sm}^{3+}$ in BCP: $x\text{Tb}^{3+}$, BCP: $y\text{Mn}^{2+}$ and BCP: $z\text{Sm}^{3+}$.

The energy transfer efficiency between the ions was also calculated from the decay lifetimes by the following equation:

$$\eta = 1 - \tau/\tau_0 \quad (2)$$

where τ and τ_0 are the lifetimes of sensitizer ions with and without the presence of an activator, respectively. The energy transfer efficiencies are also shown in Table 2.

For investigating the energy transfer mechanism from Ce^{3+} to $\text{Tb}^{3+}/\text{Mn}^{2+}/\text{Sm}^{3+}$ in BCP: $x\text{Tb}^{3+}$, BCP: $y\text{Mn}^{2+}$ and BCP: $z\text{Sm}^{3+}$, the critical distance (R_c) between sensitizer and activator needs to be calculated. According to the Dexter's theory,³⁰ there are two types of interactions between sensitizer and activator: exchange interaction and multipolar interaction. The distance between sensitizer and activator becomes increasingly shorter as the concentration of activator increases. Thus, the probability of energy transfer will increase, which will cause the concentration quenching to occur and the energy migration should be hindered. The critical distance for energy transfer between sensitizer and activator in the phosphors can be calculated by equation:³¹

$$R_c = 2(3V/(4\pi XZ))^{1/3} \quad (3)$$

where V is the volume of the unit cell, Z is the number of host cations per unit cell, and X is the total concentration of sensitizer and activator at which the emission intensity of Ce^{3+} is half the emission intensity of the sample in the absence of $\text{Tb}^{3+}/$

$\text{Mn}^{2+}/\text{Sm}^{3+}$. For BCP, V is 1163.33 \AA^3 , Z is 4. Moreover, X are 0.10, 0.07, and 0.03 for BCP: $x\text{Tb}^{3+}$, BCP: $y\text{Mn}^{2+}$ and BCP: $z\text{Sm}^{3+}$, respectively. Thus, the corresponding critical distances (R_c) were estimated to be about 17.7 \AA , 19.8 \AA , and 26.46 \AA for BCP: $x\text{Tb}^{3+}$, BCP: $y\text{Mn}^{2+}$ and BCP: $z\text{Sm}^{3+}$, respectively. These results indicate that exchange interaction is almost impossible as exchange interaction is predominant only for about 5 \AA . Therefore, the energy transfer mechanism should occur through electric multipolar interaction. According to the Dexter's multipolar interaction formula and the Reisfeld's approximation, the following relationship can be applied:^{32,33}

$$\eta_{s0}/\eta_s \propto C^{\alpha/3} \quad (4)$$

where η_{s0} and η_s are the luminescence quantum efficiency of Ce^{3+} ions without and with $\text{Tb}^{3+}/\text{Mn}^{2+}/\text{Sm}^{3+}$ ions, respectively. C is the total concentration of Ce^{3+} and $\text{Tb}^{3+}/\text{Mn}^{2+}/\text{Sm}^{3+}$ ions. The value of α can be 6, 8, and 10, corresponding to dipole–dipole, dipole–quadrupole, and quadrupole–quadrupole interactions, respectively. In addition, the ratio of quantum efficiencies can be calculated from the ratio of emission intensity by the following expression:^{34,35}

$$I_{s0}/I_s \propto C^{\alpha/3} \quad (5)$$

where I_{s0} and I_s are the emission intensity of Ce^{3+} ions without and with $\text{Tb}^{3+}/\text{Mn}^{2+}/\text{Sm}^{3+}$. The relationship between I_{s0}/I_s and $C^{\alpha/3}$ is illustrated in Fig. 7. The results show that the energy transfer from Ce^{3+} to Tb^{3+} occurs through quadrupole–quadrupole interactions, whereas the energy transfer from Ce^{3+} to $\text{Mn}^{2+}/\text{Sm}^{3+}$ occurs through dipole–dipole interactions.

Based on the abovementioned discussion, BCP can produce blue emission, the color of BCP: $x\text{Tb}^{3+}$ can turn from cyan to green, the color of BCP: $y\text{Mn}$ can shift from blue to red, and that of BCP: $z\text{Sm}$ can change from cyan to pale pink. Accordingly, co-

Table 2 Decay time values of Ce/Tb/Mn/Sm in the phosphors and efficiency of the energy transfer from Ce to the doping ions

		τ_{Ce} (ns)	$\tau_{\text{Tb}}/\tau_{\text{Mn}}/\tau_{\text{Sm}}$ (ms)	η
BCP: $x\text{Tb}$	$x = 0.03$	10.311	3.494	0.534
	$x = 0.07$	10.300	3.587	0.532
	$x = 0.10$	8.809	3.499	0.456
	$x = 0.13$	8.296	3.398	0.429
	$x = 0.15$	7.546	3.296	0.390
	$x = 0.20$	5.020	3.180	0.260
BCP: $y\text{Mn}$	$y = 0.03$	8.393	26.451	0.434
	$y = 0.07$	6.883	30.551	0.356
	$y = 0.10$	6.383	29.044	0.330
	$y = 0.13$	6.316	25.772	0.327
	$y = 0.15$	6.287	25.089	0.325
	$y = 0.20$	6.176	22.010	0.319
BCP: $z\text{Sm}$	$z = 0.03$	15.610	28.762	0.807
	$z = 0.07$	12.051	28.909	0.623
	$z = 0.10$	11.827	28.958	0.612
	$z = 0.13$	9.921	22.058	0.513
	$z = 0.15$	9.496	16.233	0.491
	$z = 0.20$	9.197	15.650	0.476



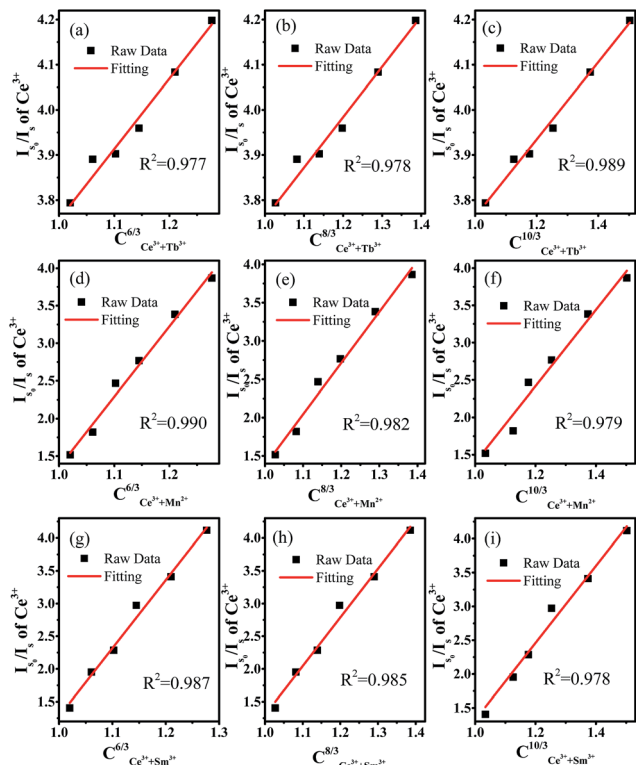


Fig. 7 (I_{510}/I_{325}) dependence on Ce^{3+} for (a–c) $C_{Ce^{3+}+Tb^{3+}}^{(6,8,10)/3}$, (d–f) $C_{Ce^{3+}+Mn^{2+}}^{(6,8,10)/3}$, (g–i) $C_{Ce^{3+}+Sm^{3+}}^{(6,8,10)/3}$.

doping Tb^{3+} and Mn^{2+}/Sm^{3+} ions in BCP may render white light. Fig. 8(A) shows the emission spectra of BCP:0.07 Tb^{3+} y Mn^{2+} . It can be seen that the characteristic peaks of Ce^{3+} , Tb^{3+} , and Mn^{2+} all appear in the spectra. Moreover, the intensity of the peaks vary with the concentration of Mn^{2+} . The inset shows the variation trend for the intensity. As the concentration of Mn^{2+} increases, the emission intensity of Ce^{3+} and Tb^{3+} all steadily decrease, whereas the emission intensity of Mn^{2+} increases at the beginning and then decreases. The decrease in the emission of Ce^{3+} is due to the energy transfer from Ce^{3+} to Tb^{3+} and Mn^{2+} , and the variation in Mn^{2+} emission is a result of concentration quenching. Moreover, the concentration quenching point for Mn^{2+} is 0.05, which is lower than that in BCP:y Mn . Thus, we considered that there may be an additional energy transfer to Mn^{2+} , as well as from Ce^{3+} . Moreover, the emission intensity of Tb^{3+} gradually decreases although there is energy transfer from Ce^{3+} to Tb^{3+} . All these results indicate that energy transfer may also occur from Tb^{3+} to Mn^{2+} in BCP:0.07 Tb^{3+} y Mn^{2+} phosphors. Moreover, as shown in Fig. 8(B), BCP:0.07 Tb^{3+} z Sm^{3+} shows a similar result to that of BCP:0.07 Tb^{3+} y Mn^{2+} . There are also emission peaks of Ce^{3+} , Tb^{3+} and Sm^{3+} , and the variation trend in the inset shows that energy can be transferred from Ce^{3+} to Tb^{3+} and Sm^{3+} . Similarly, the comparison of Sm^{3+} concentration quenching point between BCP:0.07 Tb^{3+} z Sm^{3+} and BCP:z Sm^{3+} , and the decreased emission of Tb^{3+} indicate energy transfer from Tb^{3+} to Sm^{3+} in BCP:0.07 Tb^{3+} z Sm^{3+} .

To further investigate the energy transfer from Tb^{3+} to Mn^{2+}/Sm^{3+} in BCP:0.07 Tb^{3+} y Mn^{2+} and BCP:0.07 Tb^{3+} z Sm^{3+} , the decay

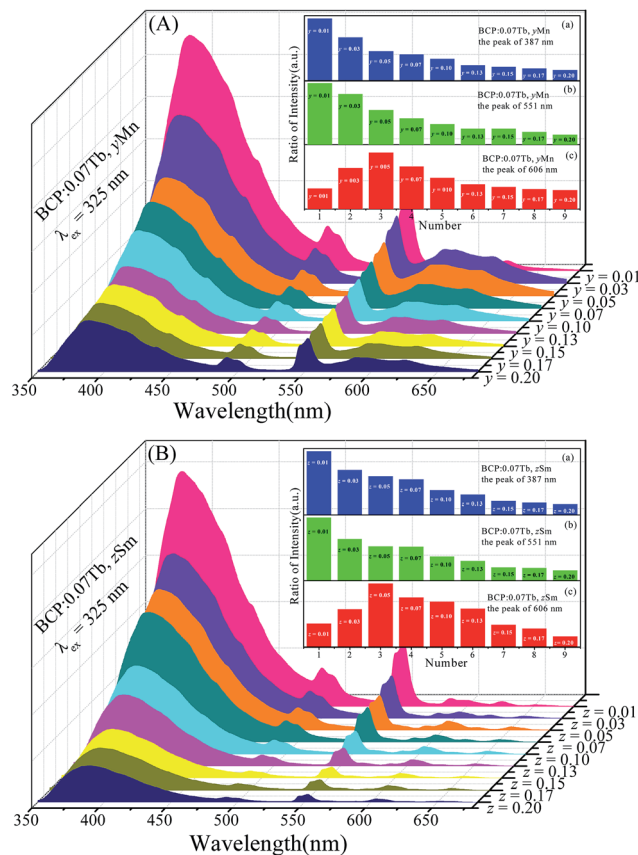


Fig. 8 ((A) and (B)) Emission spectra of BCP:0.07 Tb ,y Mn and BCP:0.07 Tb ,z Sm ; the insets of (A) and (B) are the corresponding ratios of peak intensities at 387 nm, 551 nm, and 606 nm.

curves of Tb^{3+} ($\lambda_{em} = 551$ nm, $\lambda_{ex} = 377$ nm), Mn^{2+} ($\lambda_{em} = 606$ nm, $\lambda_{ex} = 387$ nm), and Sm^{3+} ($\lambda_{em} = 606$ nm, $\lambda_{ex} = 387$ nm) were obtained and are plotted in Fig. 9. The corresponding decay time values, calculated by formula (1), are listed in Table 3. Upon comparing the decay time values in Table 3 with the values in Table 2, we found significant differences. First, the decay time of Tb^{3+} in BCP:0.07 Tb^{3+} is 3.587 ms. On the other hand, the decay time of Tb^{3+} in both BCP:0.07 Tb^{3+} y Mn^{2+} and BCP:0.07 Tb^{3+} z Sm^{3+} decreases as the concentration of doping ion increases. Moreover, we found that the decay time values of Mn^{2+} in BCP:0.07 Tb ,y Mn^{2+} are also greater than those in BCP:y Mn^{2+} at the same concentration of Mn^{2+} , which is also the same for the decay time values of Sm^{3+} . Based on these results, we can confirm that there is energy transfer from Tb^{3+} to Mn^{2+}/Sm^{3+} . Moreover, the decay time of Mn^{2+}/Sm^{3+} all increase at the beginning, reach a maximum at the concentration of 0.07, and thereafter decrease, which is consistent with the variation in emission intensity in Fig. 8. The change in the Mn^{2+}/Sm^{3+} decay time is a combination of energy transfer from Ce^{3+}/Tb^{3+} to the doping ions and concentration quenching. Moreover, we also calculated the decay time values of Ce^{3+} ($\lambda_{em} = 325$ nm, $\lambda_{ex} = 387$ nm) in BCP:0.07 Tb^{3+} y Mn^{2+} and BCP:0.07 Tb^{3+} z Sm^{3+} , and found that the values are all smaller than in BCP:x Tb^{3+} , BCP:y Mn^{3+} , or BCP:z Sm^{3+} at the same concentration of doping ions, further verifying the energy transfer from Ce^{3+} to $Tb^{3+}/Mn^{2+}/Sm^{3+}$. Fig. 10 shows the energy transfer



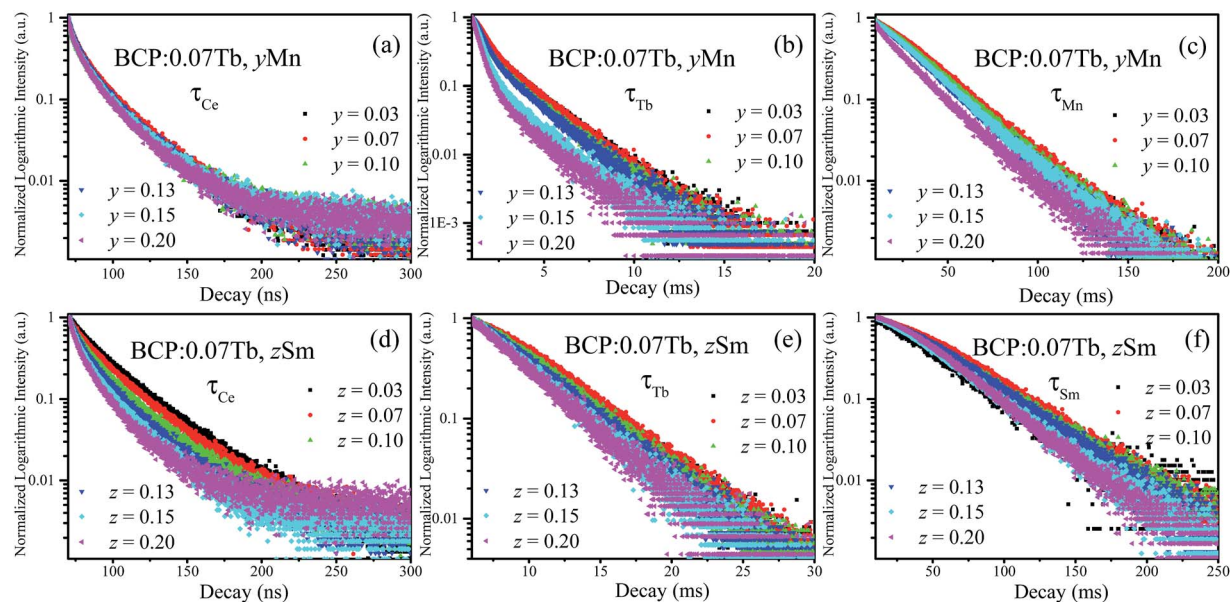


Fig. 9 (a–c) Decay curves of Ce^{3+} , Tb^{3+} , and Mn^{2+} in BCP:0.07Tb,yMn; (d–f) decay curves of Ce^{3+} , Tb^{3+} , and Sm^{3+} in BCP:0.07Tb,zSm.

relationship among the ions in BCP:0.07Tb $^{3+}$,yMn $^{2+}$ and BCP:0.07Tb $^{3+}$,zSm $^{3+}$.

3.3 CIE coordinates

The CIE chromaticity coordinates and the corresponding images of BCP:0.07Tb $^{3+}$,yMn $^{2+}$ and BCP:0.07Tb $^{3+}$,zSm $^{3+}$ are shown in Fig. 11, along with the images of BCP:xTb $^{3+}$, BCP:yMn $^{2+}$ and BCP:zSm $^{3+}$. The emitting colour can turn from blue to red by adjusting the concentration of Mn $^{2+}$ in BCP:yMn $^{2+}$. Moreover, the colour of BCP:zSm $^{3+}$ can change from cyan to pale pink, and the colour can vary from cyan to green in BCP:xTb $^{3+}$. In other words, we obtained a series of different emission colours while co-doping the host with ions at different concentrations. More importantly, the CIE chromaticity coordinates (x , y) for BCP:0.07Tb $^{3+}$,yMn $^{2+}$ excited at 365 nm vary from (0.2200, 0.3010) to (0.5143, 0.3163), with white emission of BCP:0.07Tb $^{3+}$,0.07Mn $^{2+}$. Moreover, the CIE chromaticity coordinates (x , y) for BCP:0.07Tb,zSm $^{3+}$ vary from (0.1995, 0.2893) to (0.4187, 0.2302), with white emission of

BCP:0.07Tb $^{3+}$,0.05/0.07Sm $^{3+}$. Therefore, we obtained white emission *via* co-doping Tb $^{3+}$ and Mn $^{2+}$ /Sm $^{3+}$ in BCP. Additionally, the correlated colour temperatures of BCP:0.07Tb $^{3+}$,0.07Mn $^{2+}$, and BCP:0.07Tb $^{3+}$,0.05/0.07Sm $^{3+}$ were determined to be 3812, 3196, and 3301 K, respectively, with a quantum efficiency of up to 47.9%, 48.6%, and 51.2%, respectively.

3.4 Thermal quenching properties

Thermal stability is an important parameter for phosphors as it can affect the color rendering and emission intensity. To investigate the effect of temperature on luminescence properties, the temperature-dependent emission spectra of BCP:0.07Tb,0.07Mn and BCP:0.07Tb,0.07Sm were obtained and are shown in Fig. 12(a) and (b), where the insets show that the emission intensity depends on the temperature. It is obvious

Table 3 Decay time values of Ce/Tb/Mn/Sm in the phosphors

		τ_{Ce} (ns)	τ_{Tb} (ms)	$\tau_{\text{Mn}}/\tau_{\text{Sm}}$ (ms)
BCP:0.07Tb,yMn	y = 0.03	4.505	1.455	34.666
	y = 0.07	4.330	1.334	36.495
	y = 0.10	4.155	1.153	35.344
	y = 0.13	3.757	1.126	33.073
	y = 0.15	3.509	0.777	32.372
	y = 0.20	3.406	0.576	25.810
BCP:0.07Tb,zSm	z = 0.03	8.615	2.656	48.238
	z = 0.07	6.800	2.173	54.133
	z = 0.10	6.028	2.139	46.310
	z = 0.13	5.523	2.043	41.372
	z = 0.15	4.481	2.001	40.535
	z = 0.20	3.878	1.912	40.337

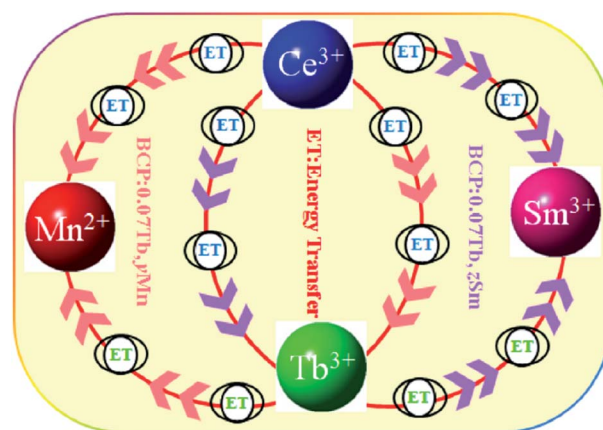


Fig. 10 Schematic of the energy transfer relationship among the ions in the phosphors.



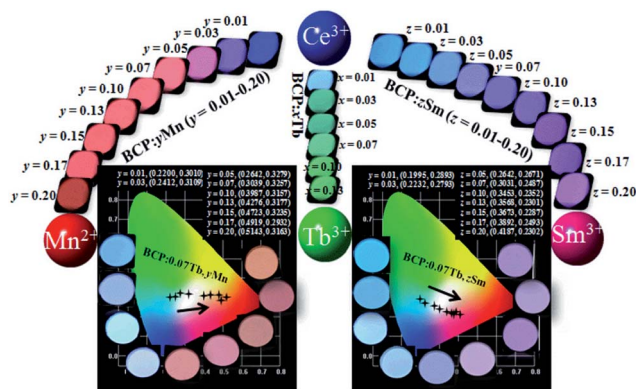


Fig. 11 CIE chromaticity coordinates and the corresponding images of the BCP:0.07Tb³⁺, yMn²⁺ and BCP:0.07Tb³⁺, zSm³⁺ phosphors. The images of BCP:yMn can be found at the left, at the right are the images of BCP:zSm, and the images of BCP:xTb are in the middle.

that the emission of Ce³⁺ in BCP:0.07Tb³⁺, 0.07Mn²⁺ and BCP:0.07Tb³⁺, 0.07Sm³⁺ decreases as the temperature increases. By contrast, the emission intensity of Tb³⁺ and Mn²⁺/Sm³⁺ in the phosphors first increases up to a maximum and then decreases. Generally, the emission intensity decreases as temperature increases due to the increase in thermal activation through the crossing point between the ground state and the excited

state.^{36,37} In our study, the increase in Tb³⁺ and Mn²⁺/Sm³⁺ emission intensity may be the result of energy transfer from Ce³⁺ to the other ions. In other words, the energy transfer efficiency from Ce³⁺ to the doping ions increases with temperature.³⁸ Fig. 12(e) shows the temperature-dependent emission spectra of BCP, where the emission intensity also decreases with temperature. Moreover, we compared the emission intensity of Ce³⁺ in BCP, BCP:0.07Tb, 0.07Mn and BCP:0.07Tb, 0.07Sm at various temperatures, as shown in Fig. 12(f). We can see that the emission intensity of Ce³⁺ in BCP is higher than that in the co-doped samples at all temperatures, which is due to energy transfer from Ce³⁺ to the doping ions. The results suggest that Ce³⁺ may transfer more energy to the ions in the host at higher temperatures. The activation energy for thermal quenching was calculated by the Arrhenius equation:^{39,40}

$$\ln(I_0/I) = \ln A - E_a/KT \quad (6)$$

where I_0 and I are the emission intensity of the phosphors at room temperature and at the experimental temperature, respectively; K is the Boltzmann constant (8.626×10^{-5} eV); A is a constant; and E_a is the activation energy for thermal quenching. Based on the abovementioned equation, the fitting curve of $\ln[(I_0/I) - 1]$ versus $1/KT$ was drawn and illustrated in Fig. 12(c) and (d). The calculated values of E_a were determined to be 0.2595 eV and 0.2346 eV for BCP:0.07Tb³⁺, 0.07Mn²⁺ and BCP:0.07Tb³⁺, 0.07Sm³⁺, respectively, which are higher than those for YAG:Ce³⁺ ($E_a = 0.136$ eV).⁴¹

4 Conclusions

In summary, we synthesized a series of BCP:xTb³⁺, BCP:yMn²⁺, and BCP:zSm³⁺ phosphors and investigated their luminescence properties. The energy transfer from Ce³⁺ to Tb³⁺/Mn²⁺/Sm³⁺ occurs in BCP:xTb³⁺, BCP:yMn²⁺, and BCP:zSm³⁺ via quadrupole-quadrupole, dipole-dipole, and dipole-dipole interactions, respectively, with a tunable color. More importantly, when co-doped Tb³⁺ and Mn²⁺/Sm³⁺ in BCP, the energy of Ce³⁺ can not only transfer to Tb, but also to Mn/Sm³⁺. Moreover, Tb³⁺ can also transfer part of its energy to Mn²⁺/Sm³⁺ in the phosphors. Above all, we obtained a white emission based on the energy transfer among the ions, and the correlated color temperatures can reach up to about 3200 K, and the quantum efficiency can be as high as 52%. In summary, the results show that we managed to obtain white phosphors by co-doping a Ba₃Ce(PO₄)₃ host with Tb³⁺ and Mn²⁺/Sm³⁺.

Acknowledgements

This work was supported by the National Natural Science Foundation of China (No. 50902042; 51672066), the Funds for Distinguished Young Scientists of the Hebei Province, China (No. A2015201129), the Natural Science Foundation of the Hebei Province, China (No. A2014201035, E2014201037), the Education Office Research Foundation of the Hebei Province, China (No. ZD2014036, QN2014085), the China Postdoctoral Science Foundation funded project (No. 2015M581311), the

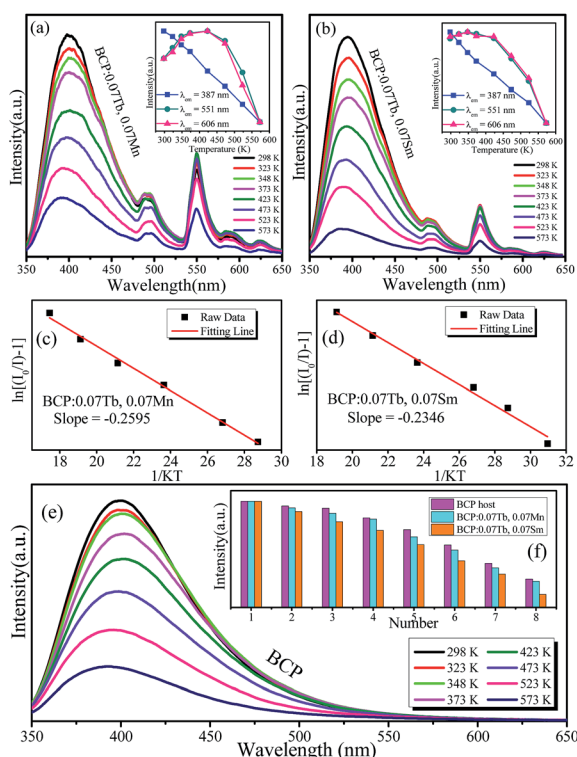


Fig. 12 (a) and (b) Temperature-dependent emission spectra of BCP:0.07Tb, 0.07Mn and BCP:0.07Tb, 0.07Sm; insets show the changes in emission intensity with temperature of the corresponding ions. (c) and (d) Activation energies of the phosphors. (e) Temperature-dependent emission spectra of BCP; the inset shows a comparison of the emission intensity of BCP, BCP:0.07Tb, 0.07Mn and BCP:0.07Tb, 0.07Sm at every temperature. (f) Comparison of the emission intensity of BCP, BCP:0.07Tb, 0.07Mn and BCP:0.07Tb, 0.07Sm at every temperature.



personnel training project of the Hebei Province, China (No. A2016002013), and the Post-graduate's Innovation Fund Project of the Hebei University (No. X2016064, X2016063).

Notes and references

- 1 P. F. Smet, A. B. Parmentier and D. Poelman, *J. Electrochem. Soc.*, 2011, **158**, R37–R54.
- 2 C. C. Lin and R. S. Liu, *J. Phys. Chem. Solids, Lett. Sect.*, 2011, **2**(11), 1268–1277.
- 3 L. Chen, C. C. Lin, C. W. Yeh and R. S. Liu, *Materials*, 2010, **3**(3), 2172–2195.
- 4 N. C. George, K. A. Denault and R. Seshadri, *Annu. Rev. Mater. Res.*, 2013, **43**, 481–501.
- 5 Z. G. Xia and R. S. Liu, *J. Phys. Chem. C*, 2012, **116**, 15604–15609.
- 6 G. Y. Lee, J. Y. Han, W. B. Im, S. H. Cheong and D. Y. Jeon, *Inorg. Chem.*, 2012, **51**(20), 10688–10694.
- 7 H. S. Roh, S. Hur, H. J. Song, I. J. Park, D. K. Yim, D. W. Kim and K. S. Hong, *Mater. Lett.*, 2012, **70**(3), 37–39.
- 8 V. Bachmann, C. Ronda and A. Meijerink, *Chem. Mater.*, 2009, **21**, 2077–2084.
- 9 S. Ye, F. Xiao, Y. X. Pan, Y. Y. Ma and Q. Y. Zhang, *Mater. Sci. Eng., R*, 2010, **71**(1), 1–34.
- 10 W. R. Liu, C. H. Huang, C. W. Yeh, J. C. Tsai, Y. C. Chiu, Y. T. Yeh and R. S. Liu, *Inorg. Chem.*, 2012, **51**, 9636–9641.
- 11 R. Yu, H. M. Noh, B. K. Moon, C. C. Byung, H. J. Jung, J. Kiwan, S. Y. Soung and K. J. Jun., *J. Alloys Compd.*, 2013, **576**(29), 236–241.
- 12 C. C. Zhao, X. Yin, Y. M. Wang, F. Q. Huang and Y. Hang, *J. Lumin.*, 2012, **132**(3), 617–621.
- 13 W. Zhou, D. Hou, F. Pan, B. Zhang, P. Dorenbos, Y. Huang, Y. Tao and H. Liang, *J. Mater. Chem. C*, 2015, **3**, 9161–9169.
- 14 J. He, R. Shi, M. G. Brik, P. Dorenbos, Y. Huang, Y. Tao and H. Liang, *J. Lumin.*, 2015, **161**, 257–263.
- 15 D. Hou, C. Liu, X. Kuang and H. Liang, *Opt. Express*, 2012, **20**(27), 28969–28980.
- 16 L. Zhou, H. Liang, P. A. Tanner, S. Zhang, D. Hou, C. Liu and L. Li, *J. Mater. Chem. C*, 2013, **1**(43), 7155–7165.
- 17 T. Sheng, Z. Fu, X. Wang, S. Zhou, S. Zhang and Z. Dai, *J. Phys. Chem. C*, 2012, **116**(36), 19597–19603.
- 18 C. H. Huang, L. Y. Luo and T. M. Chen, *J. Electrochem. Soc.*, 2011, **158**, J341–J344.
- 19 C. H. Hsu and C. H. Lu, *J. Mater. Chem.*, 2011, **21**(9), 2932–2939.
- 20 T. Li, P. L. Li, Z. J. Wang, S. C. Xu, Q. Y. Bai and Z. P. Yang, *RSC Adv.*, 2015, **5**, 71735–71742.
- 21 N. Guo, Y. Jia, W. Lu, W. Lv, Q. Zhao, M. Jiao, B. Shao and H. You, *Dalton Trans.*, 2013, **42**, 5649–5654.
- 22 Z. Wang, S. Lou and P. Li, *J. Lumin.*, 2014, **156**, 87–90.
- 23 N. Guo, Y. Huang, Y. Jia, W. Lv, Q. Zhao, W. Lü, Z. Xia and H. You, *Dalton Trans.*, 2013, **42**(4), 941–947.
- 24 H. P. Ji, Z. H. Huang, Z. G. Xia, M. S. Molokeev, X. X. Jiang, Z. S. Lin and V. V. Atuchin, *Dalton Trans.*, 2015, **44**, 7679–7686.
- 25 T. Li, P. L. Li, Z. J. Wang, S. C. Xu, Q. Y. Bai and Z. P. Yang, *Inorg. Chem.*, 2016, **55**, 8758–8769.
- 26 C. Wang, P. L. Li, Z. J. Wang, Y. S. Sun, J. G. Cheng, Z. L. Li, M. M. Tian and Z. P. Yang, *Phys. Chem. Chem. Phys.*, 2016, **18**, 28661–28673.
- 27 Y. Jia, H. Qiao, Y. Zheng, N. Guo and H. You, *Phys. Chem. Chem. Phys.*, 2012, **41**, 3537–3542.
- 28 N. Guo, H. P. You, Y. H. Song, M. Yang, K. Liu, Y. H. Zheng, Y. J. Huang and H. J. Zhang, *J. Mater. Chem.*, 2010, **20**, 9061–9067.
- 29 F. Xiao, E. H. Song and Q. Y. Zhang, *Spectrochim. Acta, Part A*, 2014, **122**, 343–347.
- 30 D. L. Dexter and J. H. Schulman, *J. Chem. Phys.*, 1954, **22**(6), 1063–1070.
- 31 D. L. Dexter, *J. Chem. Phys.*, 1953, **21**(5), 836–850.
- 32 R. Reisfeld, E. Greenberg, R. Velapoldi and B. Barnett, *J. Chem. Phys.*, 1972, **56**(4), 1698–1705.
- 33 C. H. Huang, T. W. Kuo and T. M. Chen, *ACS Appl. Mater. Interfaces*, 2010, **2**(5), 1395–1399.
- 34 K. H. Kwon, W. B. Im, H. S. Jang, H. S. Yoo and D. Y. Jeon, *Inorg. Chem.*, 2009, **48**(11), 11525–11532.
- 35 P. Paulose, G. Jose, V. Thomas, N. Unnikrishnan and M. Warriar, *J. Phys. Chem. Solids*, 2003, **64**(5), 841–846.
- 36 K. Li, M. J. Xu, J. Fan, M. M. Shang, H. Z. Lian and J. Lin, *J. Mater. Chem. C*, 2015, **3**, 11618–11628.
- 37 Y. P. Varshini, *Physica*, 1967, **34**(1), 149–154.
- 38 C. Wang, P. L. Li, Z. J. Wang, Y. S. Sun, J. G. Cheng, Z. L. Li, M. M. Tian and Z. P. Yang, *Phys. Chem. Chem. Phys.*, 2016, **18**, 28661–28673.
- 39 W. Lv, Y. Jia, Q. Zhao, M. Jiao, B. Shao, W. Lü and H. You, *Adv. Opt. Mater.*, 2013, **2**(2), 183–188.
- 40 Y. H. Chen, B. Liu, C. S. Shi, G. H. Ren and G. Zimmerer, *Nucl. Instrum. Methods Phys. Res.*, 2005, **537**(1–2), 31–35.
- 41 Y. F. Zhang, L. Li, X. S. Zhang and Q. Xi, *J. Rare Earths*, 2008, **26**, 446–449.

